17th Brazilian Congress of Thermal Sciences and Engineering
November 25th-28th, 2018, Águas de Lindóia, SP, Brazil

ENCIT-2018-0765
NUMERICAL STUDY OF THE FLOW AROUND A CIRCULAR BODY INSERTED IN A WIND TUNNEL FOR LOW NUMBERS OF REYNOLDS

Leonardo Fonseca Lana
Pontifícia Universidade Católica de Minas Gerais – Dom José Gaspar Av., 500, Coração Eucarístico, Belo Horizonte, MG, Brazil
leolana88@yahoo.com.br

Cristiana Brasil Maia
Pontifícia Universidade Católica de Minas Gerais – Dom José Gaspar Av., 500, Coração Eucarístico, Belo Horizonte, MG, Brazil
cristiana@pucminas.br

Abstract. *The present paper aimed at the numerical analysis of the flow around a cylindrical body immersed in an airstream inside a wind tunnel. The simulation was performed using the commercial software Ansys - CFX ® 17.0 with the k-ω SST turbulence model. The physical parameters considered in the study were taken from the existing wind tunnel of Pontifícia Universidade Católica de Minas Gerais. The analysis was computed according to the pressure and friction coefficients, pressure and velocity fields, streamlines and shear stress. The separation angle, about 80°, as well as the velocity and pressure properties of the flow in the stagnation point and in the detachment region, are in accordance with the theory. While in the stagnation point the pressure was maximum and the velocity was null, after the separation the flow assumed low ranges of pressure and greater velocities. Finally, the wake presented lower speeds due to the vortex formation.*

Keywords: wind tunnel, turbulence, flow around a circular cylinder, CFD

1. INTRODUCTION

Scientific advances are made throughout history by observations of routine phenomena or of those that had not been identified before. When the subject is flow, the knowledge and understanding of the basic principles and concepts of fluid mechanics is essential for the analysis of any system in which a fluid is the operating medium. The responses are applied in the creation or improvement of aerodynamic solutions of means of transportation, civil constructions or flow machines (White, 2009).

A branching of fluid mechanics corresponds to aerodynamics. Its purpose is to study the flow of a gaseous fluid around bodies or internally to them, aiming the identification of the forces acting on the system. In the state of dynamic equilibrium, the forces developed during the flow must be compensated by those produced by the air masses.

In this regard, wind tunnels appear as tools able to provide simulations and aerodynamic experiments. It is only through parameters and references about the behavior of the flow on solid bodies that the tests can be performed with fidelity and reliability (Çengel and Cimbala, 2006).

In parallel with the experimental analyses, CFD techniques have been widely used because they give a good approximation to the reality of the flow. In addition, they make it possible to reduce costs, space and time, once they eliminate efforts to build physical models by predicting the behavior of the fluid flowing (Versteeg and Malalasekera, 2007). However, despite the reliability and accuracy of the CFD techniques, they are not able to replace the wind tunnels completely, since it is necessary the experimental validation of the obtained results.

The flow around a cylinder inserted in the test section of a wind tunnel reproduces situations typical of the daily life, being able to be interpreted, for example, as airstreams intercepting a civil construction or marine streams passing around underwater structures, such as oil platforms or wind turbine towers.

Several studies are done aiming to analyze the flow around bodies immersed in fluids. Even so, concepts related to fluid dynamics are still quite dependent on empirical results and previous research experiences. In this context, Soares (2008) studied experimentally the fluid dynamics behavior of the test section of wind tunnel of Pontifícia Universidade Católica de Minas Gerais (PUC Minas). By using pitometry and thermal anemometry, velocity profiles were obtained at the exit of the test section for 15 different rotations of the blower, characterizing Reynolds numbers ranging from 6.32×10^4 to 1.12×10^5.

Al-Maliky (2013) investigated numerically the laminar flow around a rotating cylinder in two dimensions. As result, the lifting coefficient did not change significantly as a function of the increase in the Reynolds number, but underwent a great variation when the rate of rotation of the cylinder was changed. The analyses were done for Reynolds numbers of 200, 400, 800 and 1000.

Stringer *et al*. (2014) simulated structural loads generated by vortex shedding in cylindrical geometries through URANS equations for Reynolds number ranging from 40 to 10^6. The proposed methodology presented a high precision in both CFX and OpenFOAM software for Re $<10^3$. For larger Reynolds number, however, while OpenFOAM presented values closer to the literature for lift and drag coefficients and frequency of separation, CFX stood out in force coefficients but failed to obtain a realistic wake.

Izhar *et al*. (2017) simulated the induced vortex oscillations of a rigid circular cylinder with elastic support for Re=3800. This technique was based on the commercial solver Mechanical of the Ansys CFX software with the use of a programming solution known as FSI (fluid structure interaction). If compared the results obtained with the existing literature, the amplitude of the non-dimensional support coefficient (0.64) is smaller in relation to preliminary data (0.79). This difference was attributed to the fact that the present simulation was done in two dimensions, while other studies were done in three dimensions. If only 2D simulations were considered, the results were satisfactory for both one and two degrees of freedom.

D'Alessandro *et al*. (2016) studied numerically the evolution of vortices around a cylinder using variations of the DES model. The authors emphasized the importance of doing the mesh test to achieve a convergence such that the results are not distorted, as well as it is fundamental that the available computing resources are dimensioned for the purpose of the simulation.

With the use of Ansys CFX software, Chandran e*t al*. (2017) investigated numerically the influence of non-dimensional rotational velocity on a laminar flow with forced convection. For this study, a horizontal cylinder was used with a rotating movement, to which a constant thermal flow was applied as boundary condition. The results were computed as function of the Reynolds number (25, 30, 35 and 40) and of Prandtl number (0.7, 0.9, 1.4 and 5.4). As conclusion, the rotational effects, for a given Reynolds number, led to a reduction in heat transfer compared to a stationary cylinder, since the boundary layer thickness increased in this condition. An increase in the number of Prandtl caused the rate of heat transfer to the fluid to increase. Finally, as the speed of rotation increased, the maximum heat transfer shifted to the bottom of the cylinder along the counterclockwise direction due to redistribution of flow and thermal field.

Vasconcellos (2015) compared the results of three turbulence models for Re=$3.96\text{x}10^5$ and concluded that the k-ω SST and EASRM BSL models presented results consistent with the literature, while the standard k-ε model failed to predict some properties.

The present work aims to characterize numerically the air flow around a circular cylindrical body inserted in the test section of a wind tunnel and, therefore, to evaluate it properties for a given rotation of the blower. These studies, in addition to the existing literature, amplify the state of the art by predicting the results for a situation not yet evaluated experimentally.

2. METHODOLOGY

The equations of Fluid Mechanics provide a complete description of the fluid at each point along the time, once they consider mass transport, momentum and energy phenomena, velocity fields, distribution of forces in the fluid and the interaction of these with the walls. These equations are of the nonlinear partial differential type, which solution is complex and requires approximations to obtain a result (White, 2009).

There are some methodologies to treat turbulence, since it is not possible to determine the solution of a turbulent flow by applying the mass conservation and linear motion equations in their conventional form (Bejan, 2013). The most used method was proposed by Reynolds and states that the properties of the flow can be given by the sum of a time-weighted average, indicated under a bar, and a floating part, represented by a '. Thus, the properties can be subdivided into two components which, together, are equal to the instantaneous property, as shown in Eq. (1), for velocity, and in Eq. (2), for pressure.

$$V_i = \bar{V}_i + V_i' \tag{1}$$

$$P = \bar{P} + P' \tag{2}$$

The equation of continuity for the turbulent regime is written according to Eq. (3).

$$\frac{\partial \rho}{\partial t} + \frac{\partial(\rho \bar{u})}{\partial x} + \frac{\partial(\rho \bar{v})}{\partial y} + \frac{\partial(\rho \bar{w})}{\partial z} = 0 \tag{3}$$

The RANS equations arise from the introduction of the flotation components from Reynolds averages – Eq. (1) and Eq. (2) – and are represented by Eq. (4), Eq. (5) and Eq. (6).

$$\rho\left(\frac{\partial \bar{u}}{\partial t}+u\frac{\partial \overline{uu}}{\partial x}+v\frac{\partial \overline{uv}}{\partial y}+w\frac{\partial \overline{uw}}{\partial z}\right)= -\frac{\partial \bar{P}}{\partial x}+\mu\frac{\partial^2 \bar{u}}{\partial x^2}+\mu\frac{\partial^2 \bar{u}}{\partial y^2}+\mu\frac{\partial^2 \bar{u}}{\partial z^2}-\left[\frac{\partial\left(\rho\overline{u'^2}\right)}{\partial x}+\frac{\partial(\rho\overline{u'v'})}{\partial y}+\frac{\partial(\rho\overline{u'w'})}{\partial z}\right]+S_{Mx} \quad (4)$$

$$\rho\left(\frac{\partial \bar{v}}{\partial t}+u\frac{\partial \overline{vu}}{\partial x}+v\frac{\partial \overline{vv}}{\partial y}+w\frac{\partial \overline{vw}}{\partial z}\right)= -\frac{\partial \bar{P}}{\partial y}+\mu\frac{\partial^2 \bar{v}}{\partial x^2}+\mu\frac{\partial^2 \bar{v}}{\partial y^2}+\mu\frac{\partial^2 \bar{v}}{\partial z^2}-\left[\frac{\partial(\rho\overline{v'u'})}{\partial x}+\frac{\partial\left(\rho\overline{v'^2}\right)}{\partial y}+\frac{\partial(\rho\overline{v'w'})}{\partial z}\right]+S_{My} \quad (5)$$

$$\rho\left(\frac{\partial \bar{w}}{\partial t}+u\frac{\partial \overline{wu}}{\partial x}+v\frac{\partial \overline{wv}}{\partial y}+w\frac{\partial \overline{ww}}{\partial z}\right)= -\frac{\partial \bar{P}}{\partial z}+\mu\frac{\partial^2 \bar{w}}{\partial x^2}+\mu\frac{\partial^2 \bar{w}}{\partial y^2}+\mu\frac{\partial^2 \bar{w}}{\partial z^2}-\left[\frac{\partial(\rho\overline{w'u'})}{\partial x}+\frac{\partial(\rho\overline{w'v'})}{\partial y}+\frac{\partial\left(\rho\overline{w'^2}\right)}{\partial z}\right]+S_{Mz} \quad (6)$$

In Eq. (4), Eq. (5) and Eq. (6), ρ represents the specific mass of the fluid; t is the temporal coordinate in space; u, v and w are the components of the velocity of the flow in cartesian directions x, y and z, respectively; μ represents the dynamic viscosity of the fluid; P indicates static pressure in each direction; S_Mx, S_My, and S_Mz are the source terms due to field strengths for each direction.

Two equations turbulence models are widely used, since they confer great precision between analytical and computational calculations. For the solution of the problems, different transport equations are used, which consider speed and length scales separately (Ansys, 2013).

Among turbulence models of RANS methodology, k-ε and k-ω are highlighted. Both consider the turbulent kinetic energy (k), which property represents the variation in fluctuations in flow velocity. The difference between them is in the use of the turbulent energy dissipation rate (ε) or the dissipation frequency of turbulent kinetic energy (ω). The correlation between the models is done by Eq. (7).

$$\varepsilon = k.\omega \quad (7)$$

The most used model in the industry is the k-ε one. Ansys (2013) attributes this popularity to its low computational cost, ease implementation and operating stability. Versteeg and Malalasekera (2007), however, cite some negative points of this model, such as suppression of separation on curved surfaces in the presence of adverse pressure gradients and excessive levels of turbulence in the stagnation point, leading to a heat transfer in the regions of fluid attachment after the body.

In the k-ε model, the Reynolds stresses are modeled as a function of k and ε through the Boussinesq Hypothesis of turbulent viscosity (μ_t) – Eq. (8). C_μ is a constant of this turbulent model (C_μ=0,09).

$$\mu_t = \rho C_\mu \frac{k^2}{\varepsilon} \quad (8)$$

The k-ω model proposed by Menter incorporates two new equations, one for k – Eq. (9) – and one for ω – Eq. (10).

$$\frac{\partial(\rho k)}{\partial t}+\nabla(\rho k U)=\nabla\left[\left(\mu+\frac{\mu_t}{\sigma_k}\right)\nabla k\right]+P_k-\beta^*\rho k\omega \quad (9)$$

$$\frac{\partial(\rho\omega)}{\partial t}+\nabla\left(\rho\omega\vec{U}\right)=\nabla\left[\left(\mu+\frac{\mu_t}{\sigma_{\omega,t}}\right)\nabla\omega\right]++\gamma_2\left(2\rho S_{ij}.S_{ij}-\frac{2}{3}\rho\omega\frac{\partial U_i}{\partial x_j}\delta_{ij}\right)-\beta_2\rho\omega^2+2\frac{\rho}{\sigma_{\omega,2}\omega}\frac{\partial k}{\partial x_k}\frac{\partial \omega}{\partial x_k} \quad (10)$$

In Eq. (9) and Eq. (10), the representative constants are: σ_k=1.0, $\sigma_{\omega,1}$=2.0, $\sigma_{\omega,2}$=1.17, γ_2=0.44, β_2=0.083 and β*=0.09.

The drag force on a cylinder involves the friction factor, represented by the shear stress of the boundary layer on the surface, and the pressure in the direction of flow resulting from the formation of the wake (Incropera *et al*., 2008). The drag force is obtained by Eq. (11).

$$F_d = C_d.A_f.\frac{\rho.U_\infty^2}{2} \quad (11)$$

In Eq. (11), F_d represents the drag force, C_d is the drag coefficient, A_f is the front area of the cylinder – given by the multiplication of diameter by length – and the ratio $\frac{\rho.V_\infty^2}{2}$ corresponds to the dynamic pressure.

Another factor to be evaluated in flows around circular cylinders, according to White (2009), is the pressure coefficient (C_p), given by Eq. (12). This dimensionless parameter allows the visualization of favorable pressure gradients when the flow is descending; adverse, in the case of ascendant; null, when the profile presents minimal variations of its values. In other words, C_p provides a relation of the pressure behavior along the cylinder and allows to evaluate the separation point of the flow.

$$C_p = \frac{P - P_\infty}{\frac{1}{2}\rho.U_\infty^2} \tag{12}$$

In Eq. (12), the term $P - P_\infty$ represents the difference between the local pressure with respect to a referential point – P is the static pressure at the separation point and P_∞ is the pressure in the free flow –; ρ is the specific mass of the fluid and U_∞ is the velocity of the free flow.

The friction coefficient (C_f) is obtained by the relation between the shear stress in the cylinder wall (τ_w) and the dynamic flow pressure – Eq. (13).

$$C_f = \frac{\tau_w}{\frac{1}{2}\rho.U_\infty^2} \tag{13}$$

3. COMPUTATIONAL PROCEDURE

The simulated wind tunnel is installed in Pontifícia Universidade Católica de Minas Gerais and has a total length from the entrance to the exit of 3140 mm. The test section is squared with 200 mm of edge and 940 mm of length. A centrifugal blower is driven by a frequency inverter allowing operations with a speed range between 1800 rpm and 3200 rpm. In the present analysis, the rotation reached on the blower was 3200 rpm.

The cylinder has a diameter of 30 mm and a length of 200 mm. Aiming at a lower influence of the boundary layers of the tunnel walls, it is positioned in the center of the test section, both in the longitudinal and vertical directions, as shown in Fig. 1.

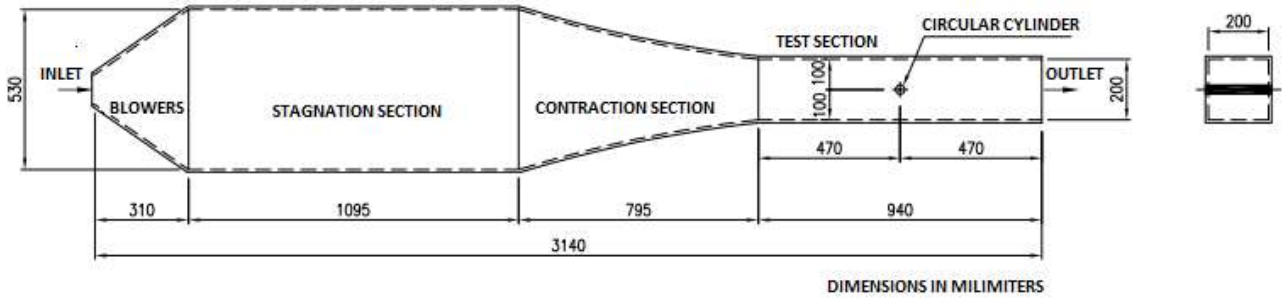

Figure 1. Simulated wind tunnel with the cylinder placed on its test section.

Experiments with Pitot tube were performed by Soares (2013) and reported that the rotation of 3200 rpm gives the fluid an average speed of 7.92 m/s at the entrance of the test section and a volumetric flow rate of 0.31 m^3/s in this same place.

The numerical analyses were performed with the commercial program Ansys CFX® 17.0 installed on a computer with Windows® Server 2012R operating system, processor Xeon E5-2660 Six-Core from Intel with 2.2 GHz of frequency, 64 GB of RAM memory and video board Nvidia Quadro M4000.

The boundary conditions and hypotheses established in the simulations were:

a) no slip condition on the walls;
b) turbulent intensity of 5% at the entrance of the test section;
c) outlet condition: tunnel outlet with static relative pressure of 0 Pa;
d) inlet condition: mass flow;
e) air as an ideal gas;
f) isothermal flow at 15 °C;
g) permanent and incompressible regime.

The numerical model of the test section of the studied wind tunnel is shown in Fig. 2.

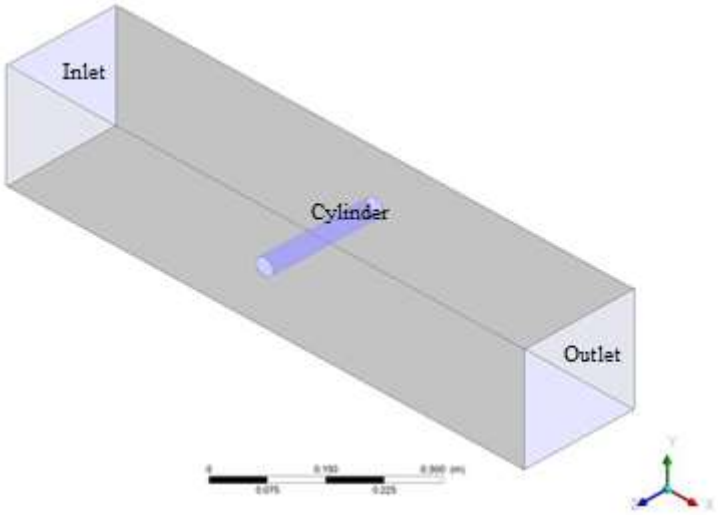

Figure 2. Numerical model of test section.

In the solution of the descriptive equations of this problem, the Reynolds number calculated for internal flow in ducts, $Re=1.08x10^5$, was based on the hydraulic diameter of the test section. Furthermore, according to Çengel and Cimbala (2006), internal flows with Re>4000 are considered turbulent. Since the Reynolds number before-mentioned is above this range, the simulations were done using the turbulence model k-ω SST.

On the other hand, if it were considered the flow around the cylinder, the Reynolds number assumes a new value ($Re=1.62x10^4$). In this case, Sumer and Fredsøe (2006) define that the fluid separation is laminar, and the wake is in the completely turbulent regime.

4. RESULTS

Studies of meshes independence and convergence were carried out and the most refined configuration obtained is shown in Fig. 3.

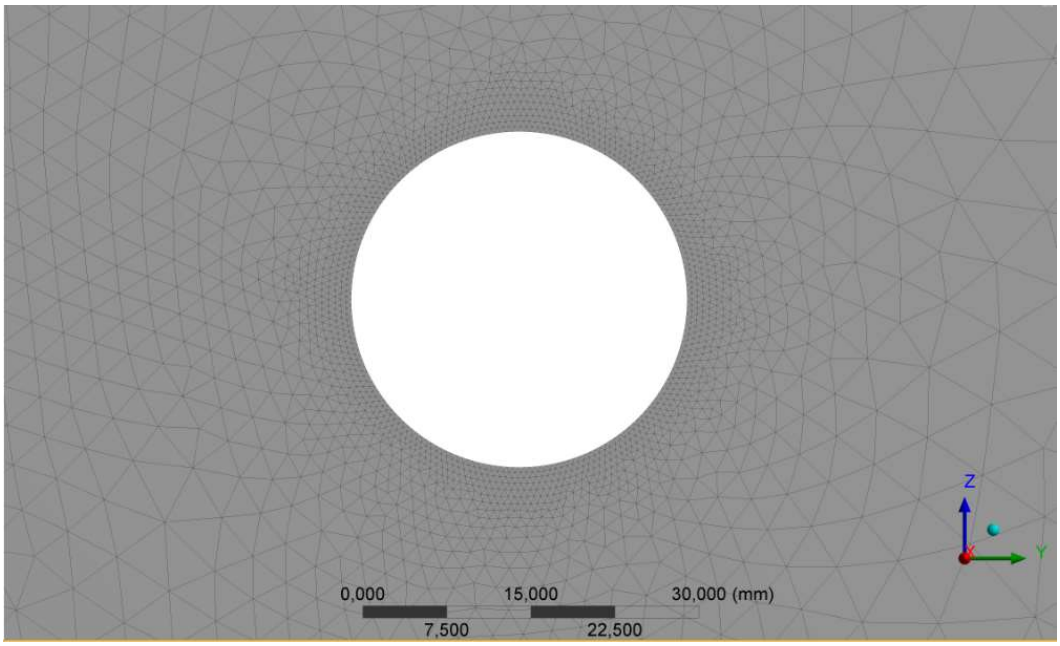

Figure 3. Mesh used in the simulations.

The mesh was considered converged when the velocity values at the evaluated points did not change more than 1% in relation to a more refined mesh for different residues (Table 1). The time required for the simulation of the converged mesh was 32 hours and 57 minutes.

Table 1. Study of meshes.

Mesh	Elements	Nodes	Convergence	Velocity (m/s)
1	245.876	93.738	10^{-4}	7,95
			10^{-5}	7,95
			10^{-6}	7,94
2	10.543.798	1.757.299	10^{-4}	7,93
			10^{-5}	7,93
			10^{-6}	7,92
3	14.678.093	2.954.765	10^{-4}	7,92
			10^{-5}	7,92
			10^{-6}	7,92

4.1 Pressure field

The pressure field taken in a plane in the center of the test section is shown in Fig. 4.

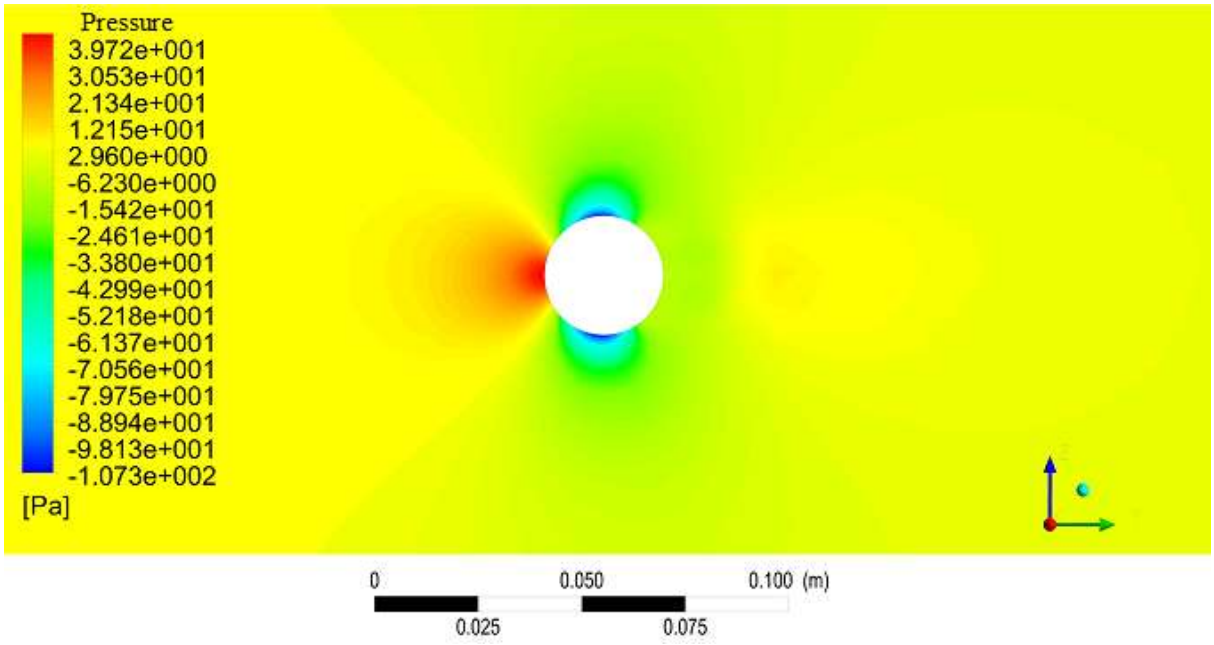

Figure 4. Pressure field around the cylinder.

The presence of a favorable pressure gradient upstream and an adverse one downstream is observed. As explained by White (2009), this negative pressure range after the cylinder is responsible for the separation of the flow and formation of the wake.

While the highest pressure computed (39.72 Pa) is at the stagnation point, the lowest value (-107.3 Pa) is in the region of separation. Thus, the pressure difference between the points upstream and downstream of the cylinder is of the order of 147.02 Pa. This variation is responsible for the existence of the drag force in the direction of the flow.

The drag force was calculated analytically using Eq. (11), with C_d=1.2 being considered for laminar flow around a cylinder, as described by Shaughnessy *et al*. (2005). The front area of the cylinder is 0.006 m^2. In this way, F_d=0.277 N.

Vasconcellos (2015) did the same analysis for 2500 rpm, in which the maximum value of 29.47 Pa was reached in the stagnation point. Moreover, in both cases the graphs profiles agree with each other.

4.2 Velocity field

The velocity field taken in a plane in the center of the test section is shown in Fig. 5.

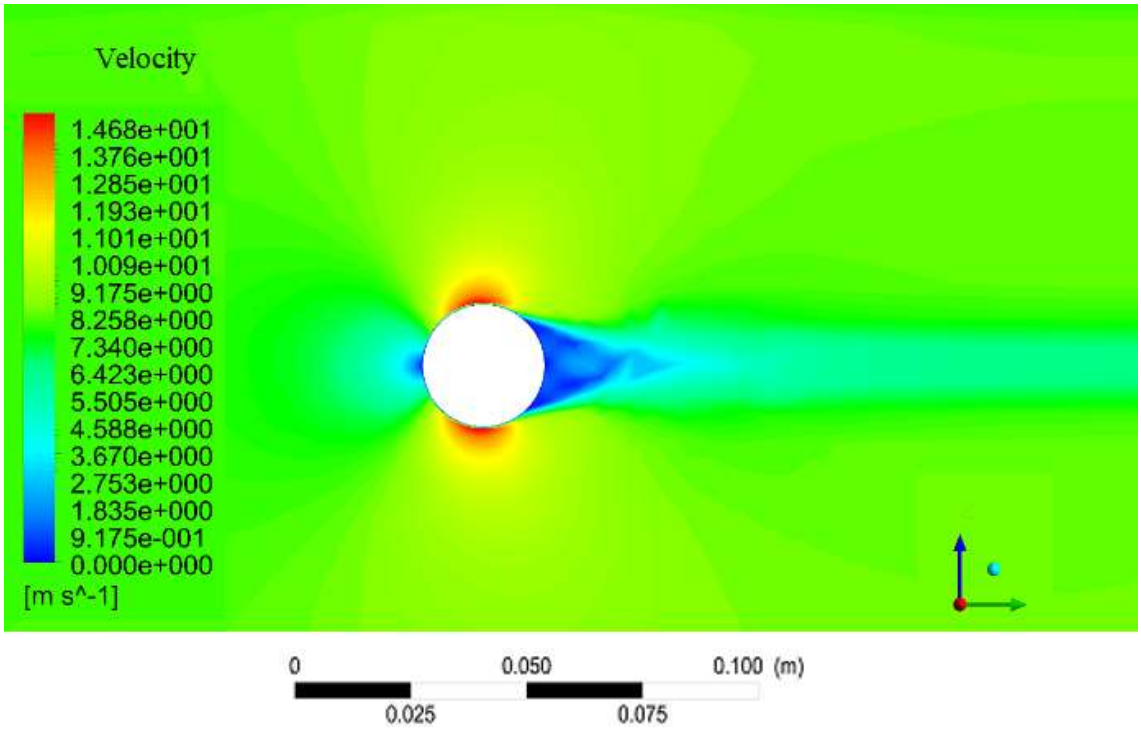

Figure 5. Velocity field around the cylinder.

In the stagnation point, the flow velocity is zero, since the fluid is brought instantaneously to rest when collides with the cylinder. In the separation region, the velocity is maximum, a characteristic explained by the fact that the friction forces with the surface of the cylinder have less influence on the flow. The maximum velocity obtained in the separation region is 14.68 m/s.

An analysis of the wake in the region immediately after the cylinder allows to observe that the fluid is at rest due to the barrier generated by the geometry of the body and to the fact that there is recirculation in that region. Thus, there is formation of internal vortex, but the flow does not advance towards the exit of the test section.

Comparing the results and the graphs profiles with those obtained by Vasconcellos (2015) at 2500 rpm, which obtained a maximum velocity at the separation point of 10.69 m/s, the values presented here are consistent.

4.3 Streamlines

The streamlines are shown in Fig. 6. As described in the velocity field, the velocity is zero at the stagnation point and in the wake region. When separating, however, this property acquires maximum value. Thus, the streamlines graph just complements what is seen in Fig. 5.

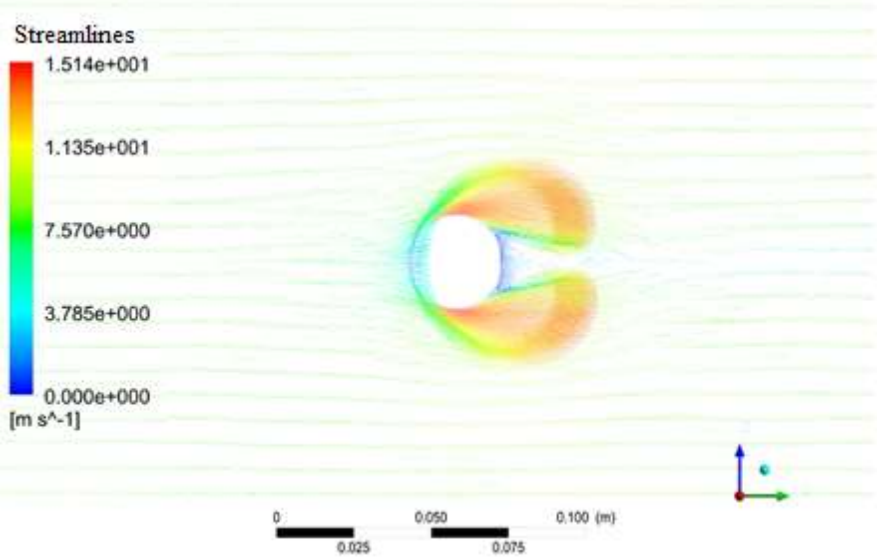

Figure 6. Streamlines around the cylinder.

4.4 Pressure coefficient

The evaluation of the pressure coefficient graph (Fig. 7) allows to identify the region of separation of the flow, which is characterized as the position of the surface of lower value for C_p. In the stagnation point, the fluid is decelerated instantaneously to rest, fact evidenced by C_p=1. The pressure gradients are identified along the surface of the cylinder and may be favorable (descending portion), adverse (ascending portion) or zero (after 120°). The small variations presented when C_p=0 can be attributed to influence of vortex formation after the cylinder.

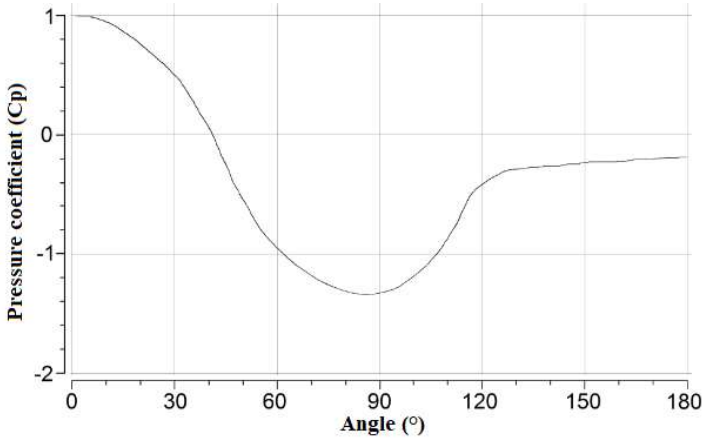

Figure 7. Pressure coefficient.

The results obtained by Vasconcellos (2015) in the separation point for a rotation of 2500 rpm, although slightly lower if compared with the present ones (approximately 70° using the turbulence model k-ω SST for this wind tunnel under the same conditions), can be considered satisfactory. The small difference is attributed to the fact that these are two independent simulations, varying the refinement of the meshes and some parameters in the data input of the program. Taking as reference the theory exposed by Shaughnessy *et al*. (2005), the separation angles are in accordance with the literature, since the authors state that the separation occurs at 82° for laminar regime.

4.5 Friction coefficient

The friction coefficient graph (Fig. 8) also makes it possible to identify the region of separation of the flow, once it occurs where the shear stress is zero. This behavior is attributed to the fact that air loses contact with the surface of the cylinder when it detaches. In the wake, the turbulence vortices create recirculation due to turbulence, causing small values of C_f.

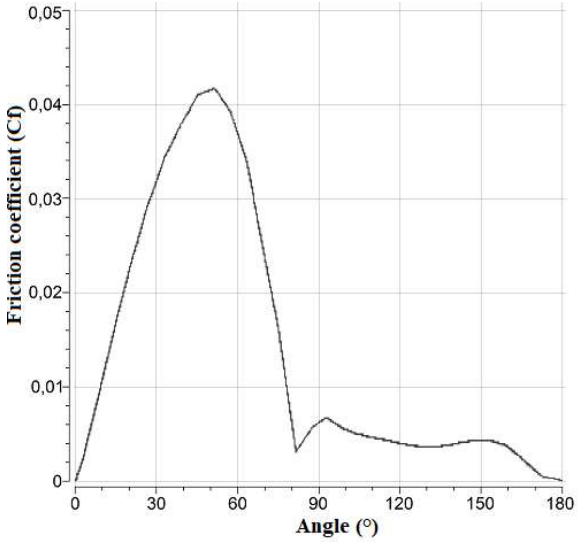

Figure 8. Friction coefficient.

The friction coefficient becomes null around 80°, a result that is consistent with that presented by the pressure coefficient curves. After detaching, the friction coefficient presents values close to zero and the instabilities in this situation are attributed to the effects of vortex formed in the wake.

Also, this result is according to that presented by Incropera *et al*. (2008), Çengel and Cimbala (2006) and Vasconcellos (2015).

4.6 Shear stress

The shear stress before the cylinder is shown in Fig. 9. For a better visualization of the behavior of this property, in Fig. 10 there is an enlarged view of the cylinder.

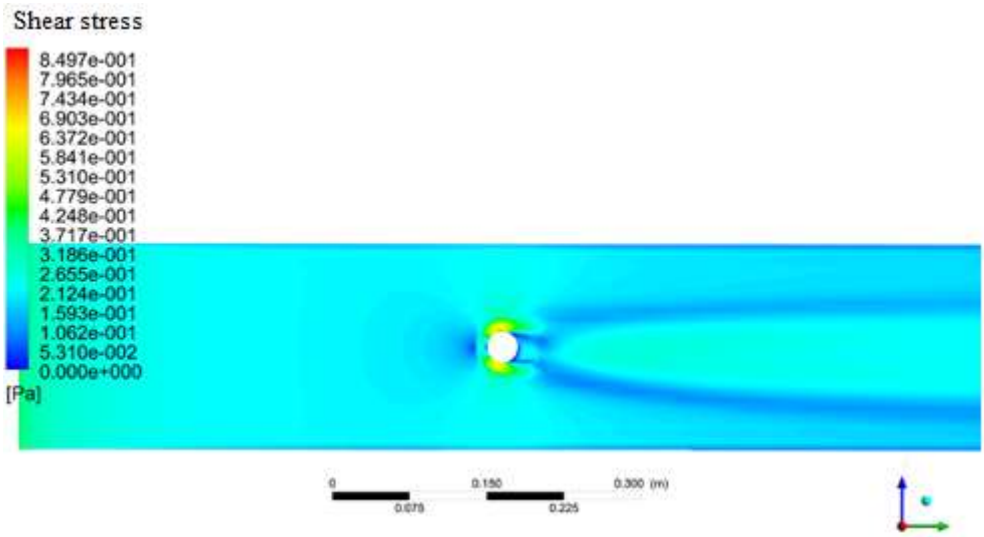

Figure 9. Shear stress around the cylinder.

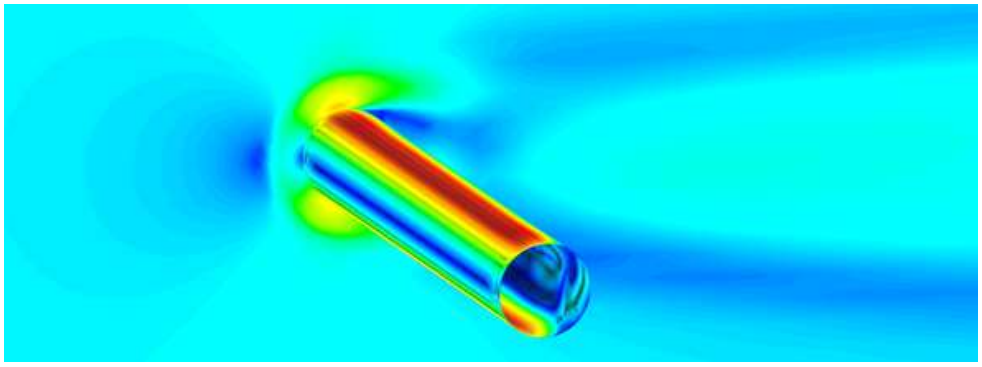

Figure 10. Enlarged view of the shear stress around the cylinder.

The behavior of the shear stress is like that one observed in the friction coefficient graph. In the region of the stagnation point, $\tau=0$, since the air collides perpendicularly to the surface of the cylinder, in order of not having influence of shear forces, only normal. When advancing in the increasing direction of the cylinder's upstream angle, this property improves gradually until it reaches its maximum value, by the separation point. After the flow is detached, the shear stress becomes zero again, since the flowing fluid stops interacting directly with the surface of the object.

5. CONCLUSIONS

This paper evaluated numerically the flow behavior around a cylinder inserted in the center of the test section of a wind tunnel for low speeds. The simulation was performed using the Ansys CFX 17.0 commercial software with the κ-ω SST turbulence model. Favorable pressure gradients before the cylinder and adverse pressure gradients after the body were observed, causing the detachment of the flow and the formation of a wake. The separation point occurred at an angle of approximately 80°. While the highest pressure was obtained in the stagnation point (39.72 Pa), the velocity in this place was zero. In the region of the separation of the flow, however, the velocity was maximum (14.68 m/s) and the pressure, minimum (-107.3 m/s).

The velocity gradients, together with the streamlines, showed the sudden resting of the fluid when it hits the cylinder in the stagnation point. In the wake, the flow goes at lower speeds compared to the rest of the test section of the wind tunnel, since the flow is diverted as it passes through the cylinder and there is vortex formation. The friction coefficient is equal to zero in the region of the detachment, fact explained by the nullity of the shear stress in this point. After about 80°, there is a certain stability. The small fluctuations that appear in this point, though, can be attributed to the vortices that arise in the region of the wake.

6. ACKNOWLEDGEMENTS

This paper was supported by Pontifícia Universidade Católica de Minas Gerais (PUC Minas), Fundação de Amparo à Pesquisa de Minas Gerais (FAPEMIG), Conselho Nacional de Desenvolvimento Científico e Tecnológico (CNPq) and Coordenação de Aperfeiçoamento de Pessoal de Nível Superior (CAPES).

7. REFERENCES

Al-Maliky, 2013. "Numerical investigation of laminar flow over a rotating circular cylinder". In *International Journal of Mechanical & Mechatronics Engineering – IJMME-IJENS,* Vol. 13, p. 32-44.

Ansys, 2013. *Ansys CFX – Solver theory guide.* ANSYS, Inc., Canonsburg, 15th edition.

Bejan, A., 2013. *Convection heat transfer.* John Wiley & Sons, Inc., Hoboken, 4th edition.

Çengel, Y. A. and Cimbala, J. M., 2006. *Fluid mechanics: fundamentals and applications*. Mcgraw-Hill, New York, 1st edition.

Chandran, P., Venugopal, G., Jaleel, H. A. and Rajkumar, M. R., 2017. "Laminar forced convection from a rotating horizontal cylinder in cross flow. In *Journal of Thermal Science*, Vol. 26, p. 153-159.

D'Alessandro, V., Montelpare, S. and Ricci, R., 2016. "Detached-eddy simulations of the flow over a cylinder at Re=3900 using OpenFOAM. In *Computers & Fluids,* Vol. 136, p. 152-169.

Incropera, F. P., Dewitt, D. P., Bergman, T. L. and Lavine, A. S., 2008. *Fundamentos de transferência de calor e massa.* LTC, Rio de Janeiro, 6th edition.

Izhar, A., Qureshi, A. H. and Khushnood, S. "Simulation of vortex-induced vibrations of a cylinder using ANSYS CFD rigid body solver". In *China Ocean Engineering,* Vol. 31, p. 79-90.

Shaughnessy, E. J., Katz, I. M. and Schaffer J. P., 2005. *Introduction to fluid mechanics.* Oxford University Press, Inc., New York.

Soares, C. B., 2008. *Estudo experimental do comportamento fluidodinâmico na seção de testes de um túnel de vento para baixas velocidades.* M. Sc. thesis, Pontifícia Universidade Católica de Minas Gerais, Belo Horizonte.

Soares, C. B., 2013. *Efeito de atenuadores passivos em flutuações de velocidade e pressão em túnel de vento.* D. Sc. thesis, Pontifícia Universidade Católica de Minas Gerais, Belo Horizonte.

Stringer, R. M., Zhang, J. and Hillis, A. J., 2014. "Unsteady RANS computations of flow around a circular cylinder for a wide range of Reynolds numbers. In *Ocean Engineering*, Vol. 87, p. 1-9.

Sumer, B. M and Fredsøe, J. *Hydrodynamics around cylindrical structures.* World Scientific, Singapore.

Vasconcellos, G. L. F., 2015. *Estudo numérico e experimental do escoamento ao redor de um cilindro circular em um túnel de vento para baixas velocidades*. M. Sc. thesis, Pontifícia Universidade Católica de Minas Gerais, Belo Horizonte.

Versteeg, H. K. and Malalasekera, W., 2007. *An introduction to computational fluid dynamics: the finite volume method*. Pearson Educational Limited, Harlow, 2nd edition.

White, F. M., 2009. *Fluid mechanics*. Mcgraw-Hill, New York, 7th edition.

8. RESPONSIBILITY NOTICE

The authors are the only responsible for the printed material included in this paper.